

# On the Antenna Pattern of an Orbiting Interferometer

Giacomo Giampieri\*

*Jet Propulsion Laboratory, California Institute of Technology, Pasadena, California, 91109*

(March 1997)

## Abstract

The response of an interferometer changing its orientation with respect to a fixed reference frame is analyzed in terms of the beam-pattern factors and the polarization-averaged antenna power pattern. Given the antenna's motion, the latter quantity describes the antenna's directionality as a function of time.

An interesting case is represented by the class of motions where the detector's plane is constrained to move on the surface of a cone of constant aperture; at the same time, the two arms are rotating around a vertical axis. This picture describes, in particular, the motion of LISA, a proposed space-based laser interferometer, as well as of other planned missions. The overall sky's coverage, and that of the galactic plane in particular, is provided as a function of the cone's aperture.

Similarly, one can consider the case of an earth-based interferometer. Using the same formalism, one can derive a simple expression for the antenna pattern, averaged over the time of arrival of the signal, as a function of the position and orientation on the earth's surface. In particular, there turn out to be two particular values for the terrestrial latitude and the inclination angle with respect to the local parallel which render the time-averaged antenna response perfectly isotropic.

In the frequency domain, the general result is that the detector's motion introduces in the instrumental response to a long-duration continuous signal a few harmonics of the orbital frequency, whose magnitude depends on the source's position in the sky. In particular, we describe LISA's response to circularly polarized sinusoidal waves coming from a few known binary systems in our Galaxy.

PACS numbers: 04.80.Cc, 04.80.Nn, 95.55.Ym

Typeset using REVTeX

---

\*Present address: Queen Mary and Westfield College, Astronomy Unit, London E1 4NS.

## I. INTRODUCTION

Gravitational waves in the low-frequency regime ( $10^{-4}$  to  $10^{-1}$  Hz) can only be observed from space, due to terrestrial disturbances. In space, the only technique currently available, besides pulsar timing, is based on Doppler tracking of an interplanetary spacecraft [1]. However, this relatively inexpensive method has not provided enough sensitivity, thus far, for a detection. While better sensitivities may be expected in the near future, with advanced spacecraft such as CASSINI, much more ambitious projects for gravitational wave observatories in space have been proposed. Among these, the most promising detectors are based on space-born laser interferometry. In particular, LISA (Laser Interferometer Space Antenna) [2,3], and OMEGA (Orbiting Medium Explorer for Gravitational Astrophysics) [4] consist of six drag-free, laser-bearing spacecraft, launched in orbit around the sun (LISA) or the earth (OMEGA). The six spacecraft would be placed, in pair, at the vertex of a triangle with  $5 \times 10^6$  km sides for LISA, and 5 times smaller for OMEGA. At each corner, the two spacecraft are phase locked through the exchange of a laser signal, replacing in this way the central mirror of an ordinary Michelson interferometer. Each of the two probes sends a laser beam to a probe at each of the other two equilateral points, where the tracking signal is transponded back by phase-locked lasers, and the returning beams are eventually interfered.

In order to keep the triangular constellation as stable as possible, elaborated orbits have been designed. In LISA case each spacecraft is orbiting a circle of radius  $3 \times 10^6$  km over a period of 1 yr. The interferometer plane, at an inclination of  $60^\circ$  with respect to the ecliptic, is also rotating around the sun with the same periodicity. In OMEGA case the orbital plane is almost coincident with the ecliptic, and the interferometer is rotating around itself with a period of 53.21 days.

The complicate motion is reflected in the time evolution of the interferometer's response to a source located in a fixed position in the sky. We will investigate the behavior of the antenna response in presence of a generic motion, and apply our results to the specific motions of interest. As a side-product of our analysis, we can also examine a terrestrial interferometer, where the motion is simply related to the earth's rotation around its axis, and study its antenna pattern as a function of the location and orientation on the earth's surface.

In this section, we briefly recall the formalism describing the antenna response to a gravitational wave passing by, in the long-wavelength approximation [5].

First, we introduce the wave symmetric trace-free (STF) tensor

$$\mathbf{W} = h_+ \Re(\vec{m} \otimes \vec{m}) + h_\times \Im(\vec{m} \otimes \vec{m}), \quad (1)$$

where the (complex) vector  $\vec{m}$  is defined in terms of the polarization vectors  $\vec{e}_X$  and  $\vec{e}_Y$  as

$$\vec{m} = \frac{1}{\sqrt{2}} (\vec{e}_X + i\vec{e}_Y). \quad (2)$$

The tensor  $\mathbf{W}$  represents the wave field as measured in the interferometer's proper rest frame. Then we define the STF detector tensor

$$\mathbf{D} = \vec{n}_1 \otimes \vec{n}_1 - \vec{n}_2 \otimes \vec{n}_2, \quad (3)$$

where  $\vec{n}_i$  is the unit vector along the  $i$ -th arm. The interferometer response is the scalar obtained from the contraction of the wave tensor  $\mathbf{W}$  with the detector tensor  $\mathbf{D}$

$$R(t) = W_{ij}D^{ij} \equiv F_+h_+ + F_\times h_\times. \quad (4)$$

The beam-pattern factors  $F_+$  and  $F_\times$  depend on the antenna's orientation with respect to the wave's propagation direction and polarization axes.

We can choose the reference frame as in Fig. 1, with the  $x$ -axis of the  $(x, y, z)$  frame bisecting the interferometer's arms, so that the only non-null components of  $\mathbf{D}$  in this reference frame are

$$D_{12} = D_{21} = \sin(2\Omega), \quad (5)$$

where  $2\Omega$  is the aperture angle. Therefore, in order to obtain  $R(t)$ , we just need the component  $W_{12}$  in this particular frame. Fig. 1 also shows the Euler's angles  $\theta$ ,  $\phi$ , and  $\psi$  which transform from the interferometer's frame  $(x, y, z)$  to the wave reference frame  $(X, Y, Z)$ . The latter is defined with the  $Z$ -axis opposite to the propagation direction, and the  $X$  and  $Y$  axes along  $\vec{e}_X$  and  $\vec{e}_Y$ , respectively.

It is easy to find, for the  $+$  polarization

$$F_+ = \sin(2\Omega) \left[ \cos\theta \cos(2\phi) \sin(2\psi) + \frac{1}{2} (1 + \cos^2\theta) \sin(2\phi) \cos(2\psi) \right]. \quad (6)$$

The beam-pattern factor  $F_\times$  is obtained from Eq. (6) with the substitution  $\psi \rightarrow \psi + \pi/4$ , a well known polarization property of gravitational waves. However, when averages over the polarization angle  $\psi$  are considered, we can assume, without loss of generality,  $h^+ = h^\times = h$ . The quantity of interest is thus the polarization-averaged antenna's *power pattern*

$$P \equiv \left\langle \left( \frac{R}{\sin(2\Omega)h} \right)^2 \right\rangle_\psi, \quad (7)$$

which for the interferometer in Fig. 1 reads

$$P(\theta, \phi) = \frac{1}{8} \left[ 1 + \cos^4\theta + 6\cos^2\theta - \sin^4\theta \cos(4\phi) \right]. \quad (8)$$

For future reference, note that this definition of the antenna pattern is not normalized to unity, the average of  $P(\theta, \phi)$  over the whole sky being  $2/5$ . A plot of  $P(\theta, \phi)$  in polar coordinates is shown in Fig. 5a.

Eq. (8) gives the instantaneous power pattern for a wave impinging from the direction  $(\theta, \phi)$  in the interferometer's reference frame. If the detector is moving with respect to the source, then, apart from Doppler effects considerations, all we need to do is simply replace  $\theta$  and  $\phi$  with the appropriate functions  $\theta(t)$  and  $\phi(t)$ . For example, if the antenna is rotating around its vertical axis with angular velocity  $\omega$  (Fig. 2), then we can obtain the antenna pattern at any time  $t$  from Eq. (8), with the substitution

$$\phi \rightarrow \phi - \xi_0 - \omega t, \quad (9)$$

where  $\xi_0$  is some initial angle. As a matter of fact, this very simple case describes, with good approximation, the time evolution of OMEGA [4]. As mentioned in the Introduction, the idea of OMEGA is essentially similar to that of LISA, except that the six spacecraft are launched into a circular earth orbit, beyond the Moon orbit. The triangle has now  $10^6$  km sides, and it is rotating around itself with a period of  $\sim 53$  days.

However, to mask the motion of the antenna with the apparent motion of the source is not always convenient, especially when dealing with a large number of sources, or when the motion is very complicate. In this paper, we shall introduce a more useful representation, where every quantity is referred to a fixed reference frame, so that the source's polar coordinates  $\theta$  and  $\phi$  remain constant, and the antenna response depends on time through the actual motion of the interferometer.

## II. ANTENNA PATTERN FOR A GENERIC MOTION

We now introduce an arbitrary reference frame  $(x', y', z')$ , with the only requirement to be stationary with respect to fixed stars<sup>1</sup>. To be more explicit, when dealing with a space-born interferometer, we can adopt an Ecliptic coordinate system. In the last section we will also consider a terrestrial interferometer, which is most easily described in an Equatorial frame.

The full description of the antenna response requires six Euler's angles, defined as in Fig. 3. The orthogonal transformation from the wave's frame  $(X, Y, Z)$  to the fixed frame  $(x', y', z')$  is given by the orthogonal matrix

$$\mathbf{A} = \begin{pmatrix} \cos \phi \cos \psi - \cos \theta \sin \phi \sin \psi & -(\cos \phi \sin \psi + \cos \theta \sin \phi \cos \psi) & \sin \theta \sin \phi \\ \sin \phi \cos \psi + \cos \theta \cos \phi \sin \psi & -\sin \phi \sin \psi + \cos \theta \cos \phi \cos \psi & -\sin \theta \cos \phi \\ \sin \theta \sin \psi & \sin \theta \cos \psi & \cos \theta \end{pmatrix}. \quad (10)$$

The matrix  $\mathbf{B}$  which transform from  $(x, y, z)$  to  $(x', y', z')$  is analogous to the matrix  $\mathbf{A}$ , with the Euler's angles  $\theta, \phi, \psi$  replaced by the corresponding ones  $\zeta, \eta, \xi$ . Thus, the complete transformation from the wave's frame to the detector's one is given by  $\mathbf{B}^T \cdot \mathbf{A}$ . Actually, as we may expect from Fig. 3, the angles  $\phi$  and  $\eta$  appear in our results only in the combination  $\delta \equiv \phi - \eta$ .

After a rather lengthy calculation, one ends up with the following expressions for the beam-pattern factors  $F_+$  and  $F_\times$

$$F_+ = \sin(2\Omega) [A \cos(2\xi) \cos(2\psi) + B \cos(2\xi) \sin(2\psi) + C \sin(2\xi) \cos(2\psi) + D \sin(2\xi) \sin(2\psi)], \quad (11a)$$

$$F_\times = \sin(2\Omega) [B \cos(2\xi) \cos(2\psi) - A \cos(2\xi) \sin(2\psi) + D \sin(2\xi) \cos(2\psi) - C \sin(2\xi) \sin(2\psi)]. \quad (11b)$$

The coefficients  $A, B, C$ , and  $D$  in Eqs. (11) depend only on the angles  $\zeta, \theta$ , and  $\delta$ . They are explicitly given in Appendix A.

---

<sup>1</sup>Here and in the following, when we say 'stationary' (or 'fixed') we mean stationary over the characteristic time scale of the detector's motion.

We recall that the power pattern  $P$  is obtained squaring, and averaging over the polarization angle  $\psi$ , the interferometer response. From Eqs. (4), (7), and (11) we eventually obtain

$$P = \sum_{n=0}^4 \{[\lambda_n + \mu_n \cos(4\xi)] \cos(n\delta) + \sigma_n \sin(4\xi) \sin(n\delta)\} , \quad (12)$$

where now the coefficients  $\lambda_n, \mu_n$ , and  $\sigma_n$  depend only on  $\theta$  and  $\zeta$ . These coefficients, given in Appendix B, are quite complicate trigonometric polynomials of their arguments. Nonetheless, Eq. (12) turns out to be very useful in practice. In fact, for the planned detectors considered in the present paper, the angle  $\zeta$  is constant, and thus the only possible time evolution is related to the sinusoidal functions of  $\xi$  and  $\delta$  which appear explicitly in Eq. (12). Before analyzing in more detail the proposed space-born interferometers, we consider a trivial application of Eq. (12).

### A simple example

As a first test of Eq. (12) we can consider, as we did at the end of Sec. I, an interferometer which is rotating around its z-axis (see Fig. 2), so that its trivial motion is described by

$$\zeta = \eta = 0, \quad \xi = \xi_0 + \omega t . \quad (13)$$

From Eq. (13), and Eqs. (B.1)-(B.15) of Appendix B, we find that the only non-null coefficients in Eq. (12) are

$$\lambda_0 = \frac{1}{8} (1 + \cos^4 \theta + 6 \cos^2 \theta) , \quad (14)$$

$$\mu_4 = \sigma_4 = -\frac{1}{8} \sin^4 \theta , \quad (15)$$

so that

$$P = \frac{1}{8} [1 + \cos^4 \theta + 6 \cos^2 \theta - \sin^4 \theta \cos [4(\phi - \xi_0 - \omega t)]] . \quad (16)$$

As pointed out in Sec. I, this result can be obtained much more easily directly from Eq. (8), with the substitution (9). Eq. (16) gives, with good approximation, the antenna pattern of OMEGA, with  $\omega \simeq 1.4 \times 10^{-6} \text{ sec}^{-1}$ .

### III. SPACE INTERFEROMETERS: CONICAL MOTION

In the previous section, we have considered the antenna power pattern associated to an unspecified motion of the detector. We will now focus our attention to the case of a space interferometer, which presents, independently of the particular project under investigation, some very general and interesting properties.

Inserting the space interferometer in its orbit and keeping the interferometer configuration stable over the mission lifetime - at least two orbital periods - is a very demanding

navigation task, due principally to the perturbations from the earth and the other planets. For instance, one of the consequences of the complicate orbit is the fact that we cannot maintain equal distances between the probes. In a recent paper [6], we modeled the noise that is introduced into the differenced data because of the unequal arms, and showed that the final accuracy of the interferometer is not compromised. Another example of the problems we may face in a space-born interferometer is that, due to the earth disturbances, high Doppler rates would result. Hellings et al. [7] described a laser transmitter and receiver hardware system that provides the required readout accuracy and implements a self-correction procedure for the on-board frequency standard used for laser phase measurement.

We will now consider the interferometer's orbit, and discuss its implication on the antenna response to a wave coming from a given direction in the sky. In particular, as we mentioned in the Introduction, LISA [2] will orbit the sun at the earth's distance, as far behind the earth as possible. The plane containing the six probes, during its orbit, will remain always tangent to the surface of a cone of  $60^\circ$  aperture, and the detector itself will rotate in this plane with same periodicity - one year - but opposite direction. Fig. 4, reproduced from [3], shows LISA configuration.

In this section, we will consider a LISA-like motion, characterized by a generic cone aperture. In other words, the motion of each of the three interferometers is assumed to be described by<sup>2</sup>

$$\zeta = \text{const} , \tag{17a}$$

$$\eta = \eta_0 + \omega t \quad (\Rightarrow \delta = \phi - \eta_0 - \omega t) , \tag{17b}$$

$$\xi = \xi_0 - \omega t . \tag{17c}$$

Note that  $\eta$  and  $\xi$  are counter-rotating. Note also that the three interferometers formed by the triangular configuration have initial values  $\xi_0$  which differ from each other by  $120^\circ$ , whereas  $\eta_0$  is the same for all of them. For the sake of conciseness, since we are concerned here with the antenna power pattern, we will consider only one of the interferometers, leaving the possibility of exploiting the polarization sensitivity to future works.

The proposed LISA orbit has  $\zeta = 60^\circ$ , a critical value for the stability of the triangular configuration. Since the behavior of the antenna, in terms of sky's coverage, directionality, etc., is very sensitive to the inclination, we will keep  $\zeta$  as a free parameter throughout this paper, and refer to Eqs. (17) as describing a 'conical' motion. For a given  $\zeta$ , the coefficients  $\lambda_n, \mu_n$ , and  $\sigma_n$  are now functions of  $\theta$ . They are explicitly given in Appendix C for the LISA case.

In order to determine the sky's coverage during the detector's lifetime, we need to consider the time average of the antenna pattern  $P$  over one orbital period, which gives

$$\langle P \rangle_T = \lambda_0 + \frac{1}{2} (\mu_4 + \sigma_4) \cos[4(\phi - \eta_0 - \xi_0)] \tag{18}$$

---

<sup>2</sup>we could eliminate one of the two initial conditions  $\xi_0$  or  $\eta_0$  by simply rescaling the time, taking for instance the origin of time at the passage through the line of nodes ( $\xi_0 = 0$ ) or through the vernal equinox ( $\eta_0 = 0$ ).

Fig. 5 shows a plot of  $\langle P \rangle_T$  in polar coordinates for various values of the cone's aperture  $\zeta$ . Note that  $\zeta = 0$  corresponds to an interferometer fixed in space; since we are taking  $\xi$  and  $\eta$  counter-rotating, the interferometer does not rotate at all.

We know from Eq. (8) that an interferometer fixed in space can never detect waves impinging from four specific null-directions, given by  $\theta = \pi/2$ , and  $\phi = k\pi/2$  ( $k = 0, \dots, 3$ ). We can now analyze what happens to these null-directions in the generic conical case, focussing our attention to the ecliptic plane  $\theta = \pi/2$ . It is easy to show, from the behavior of the functions  $\lambda_0$  and  $|\mu_4 + \sigma_4|/2$  (see Fig. 6), that there is a tendency for the null-directions on the ecliptic plane to remain visible, although the magnitude of this effect is strongly affected by the value of  $\zeta$ : for  $\zeta = 0$  the null-directions are obviously completely preserved, while for  $\zeta = \pi/2$  the  $\phi$ -dependence is very poor. LISA is much closer to the latter case, and actually its  $\langle P \rangle_T$  is almost independent on  $\theta$  as well, as we shall see in a while.

Note that, if  $\xi$  and  $\eta$  were co-rotating, instead of counter-rotating as in LISA, then in the last term of Eq. (18) we would have to make the substitution

$$\frac{1}{2}(\mu_4 + \sigma_4) \rightarrow \frac{1}{2}(\mu_4 - \sigma_4) . \quad (19)$$

which means that the  $\phi$ -term would be even smaller, in absolute value, compared to  $\lambda_0$ .

One might infer from Fig. 5d that, if the inclination is close to  $\zeta = \pi/2$ , then the zeros of the antenna pattern can be found in the direction orthogonal to the ecliptic plane. However, this is not the case, since  $\theta = 0$  implies that  $P$  is still given by Eq. (8), with  $\theta$  and  $\phi$  replaced, respectively, by  $\zeta$  and  $\xi$ . Thus, even for  $\zeta = \pi/2$  the time average is non-zero at the poles.

Another important issue related to Eq. (18) is the time-averaged antenna directionality. As we can predict from Fig. 5, directionality is strongly dependent on the angle  $\zeta$ . To make this statement more precise, let us consider the r.m.s. deviation from isotropy, defined as

$$\Delta \equiv \left[ \frac{175}{48\pi} \int_{4\pi} (\langle P \rangle_T - 2/5)^2 d\Omega \right]^{1/2} . \quad (20)$$

The normalization factor in front of Eq. (20) is chosen in such a way that  $\Delta$  is normalized to one for a fixed interferometer. For a conical motion, inserting Eq. (18) in Eq. (20) we easily obtain  $\Delta = \Delta(\zeta)$ , shown in Fig. 7. Explicitly, we find

$$\begin{aligned} \Delta(\zeta) = \frac{1}{288} & \left[ 19779 + 120 \cos \zeta - 118380 \cos^2 \zeta \right. \\ & + 840 \cos^3 \zeta + 180690 \cos^4 \zeta + 840 \cos^5 \zeta \\ & \left. - 3180 \cos^6 \zeta + 120 \cos^7 \zeta + 2115 \cos^8 \zeta \right]^{1/2} . \end{aligned} \quad (21)$$

Thus, the antenna pattern is distributed more and more isotropically as we increase  $\zeta$  from  $\zeta = 0$ . After we reach a minimum at  $\zeta \simeq 55^\circ$ , the antenna's directionality starts increasing again.

Therefore, we can conclude that, in the conical case, it is impossible to get a perfectly isotropic response, i.e. we never get  $\Delta = 0$  (see also the above discussion about the  $\phi$ -dependence). However, we can get very close to this ideal situation, if we choose  $\zeta$  appropriately. Remarkably, LISA's inclination is very close to the optimal value  $\zeta \simeq 55^\circ$ , and

gives  $\Delta(60^\circ) \simeq 0.14$ . This means that LISA, during its lifetime, will cover the whole sky in an approximately uniform manner. Of course, in some circumstances, directionality needs to be preserved. For instance, one may want to disentangle the isotropic component of the stochastic background from the anisotropic contribution of the galactic binaries. Directionality can always be preserved integrating over a shorter period. Fig. 8 shows LISA's antenna pattern averaged over 3 and 6 months, respectively.

Finally, we want to consider the interferometer's responsiveness to the galactic plane, given that most of the strongest sources will lie on this plane. In our coordinate system, the galactic plane is characterized by

$$\theta(\phi) = \arctan(\alpha \cos \phi + \beta \sin \phi)^{-1}, \quad (22)$$

where  $\alpha \simeq 1.75$  and  $\beta \simeq 4 \times 10^{-4}$ . Assuming, for simplicity, that the sources are distributed isotropically on the plane, the event rate of disk's sources is proportional to the average area of the intersection of this plane with the antenna pattern, equal to

$$G = \frac{1}{2T} \int_0^{2\pi} \int_0^T [P(\theta(\phi), \phi)]^2 dt d\phi, \quad (23)$$

where  $\theta(\phi)$  is the function given in Eq. (22). This area depends on the details of the detector's motion, in our case on  $\zeta$ ,  $\xi_0$ , and  $\eta_0$ . Fig. 9 shows the quantity  $G$  as a function of  $\zeta$ , since the dependence on  $\xi_0$  and  $\eta_0$  can be neglected in a first approximation. For LISA, we find the small value  $G \sim 0.46$ , the exact value depending on the initial conditions  $\eta_0 + \xi_0$ . We conclude that LISA is not particularly sensitive to the galactic disk, due to the fairly large inclination to the Ecliptic of both the detector's plane and the Galaxy. According to this crude analysis, we can expect that OMEGA, with a smaller, almost negligible, inclination, would increase its chances of observing a signal from the disk by roughly a factor two. Note, however, that previous calculations [8,9] have shown that gravitational radiation from galactic binaries in the disk is comparable to that coming from the local region ( $r < 200$  pc). Since the latter is isotropically distributed, the time-varying signal from the disk contributes only a fraction of the galactic binaries stochastic background. Nonetheless, this small component could make the stochastic signal distinguishable from the detector's noise. In a future paper we will investigate the amplitude modulations introduced by the antenna motion in the confusion noise generated by different populations of galactic binary systems, and describe how to exploit this effect in order to detect the signal and to obtain information about the distribution of sources in the Galaxy.

#### IV. EARTH-BASED INTERFEROMETERS

As an additional application of Eq. (12), let us consider a terrestrial interferometer. In this case the most convenient choice for the 'fixed' reference frame is the Equatorial one, with the  $z'$  axis directed toward the North Pole, and the  $x'$  axis toward the Vernal Equinox. In this frame, the motion of the interferometer becomes similar to the conical case previously analyzed, except that now the detector can not rotate on itself, of course. In other words we have

$$\zeta = \pi/2 - \ell, \quad (24a)$$

$$\eta = \eta_0 + \omega t, \quad (24b)$$

$$\xi = \iota, \quad (24c)$$

where  $\ell$  is the terrestrial latitude,  $\omega$  is the earth's angular velocity of rotation, and  $\iota \in [-\frac{\pi}{4}, +\frac{\pi}{4}]$  is the angle between the arms' bisector and the local parallel.

For example, let us consider the average of the antenna pattern  $P$  over the time of arrival of the signal. In the terrestrial case, as opposed to the conical case considered in Sec. III, the interferometer cannot rotate around its vertical axis, and therefore averaging over time or  $\phi$  gives the same result, namely

$$\langle P \rangle_T = \lambda_0(\theta, \ell) + \mu_0(\theta, \ell) \cos(4\iota). \quad (25)$$

For any specific value of  $\theta$ , for example  $\theta = 102^\circ$ , corresponding to the direction of the center of the Virgo cluster, Eq. (25) gives the square of the r.m.s. power as a function of the antenna's position and orientation on the earth's surface, a quantity already numerically studied in [10].

Instead of fixing  $\theta$ , we could try to answer the question: is there any particular location and orientation for which the antenna pattern, averaged over one day, is isotropic? The answer turns out to be affirmative, and the isotropic antenna is characterized by

$$\ell_{is} = \arcsin\left(\pm \frac{1}{\sqrt{3}}\right) \simeq \pm 35^\circ.26438972, \quad (26a)$$

$$\iota_{is} = \frac{1}{4} \arccos\left(-\frac{1}{5}\right) \simeq \pm 25^\circ.38423976. \quad (26b)$$

One can easily check, by inspection, that  $\ell_{is}$  and  $\iota_{is}$  produce  $\langle P \rangle_T \equiv 2/5$  or, equivalently,  $\Delta \equiv 0$ . A detector located at latitude  $\ell_{is}$  and oriented by  $\iota_{is}$  maximizes the event rate of an isotropic population of sources.

In the event that the detector's position has already been chosen, one can still make use of Eq. (25) in order to find the optimal orientation  $\iota_*$  which gives the least directional antenna pattern at that latitude. At each latitude  $\ell$ , we define as optimal that orientation  $\iota_*$  which minimize the quantity  $\Delta$ . Fig. 10 shows  $\iota_* = \iota_*(\ell)$  and the corresponding minimum  $\Delta_* \equiv \Delta(\ell, \iota_*)$ .

We stress that, as one may actually expect,  $\Delta$  depends much more strongly on  $\ell$  than  $\iota$ , and in particular the antenna becomes rapidly anisotropic as we move away from  $\ell_{is}$ , no matter how optimally we try to choose  $\iota$ . Moreover, we can foresee several terrestrial interferometers to be operative in the near future, so that the sky's coverage of a single antenna is not really an issue as critical as in the space-born case previously discussed.

## V. SINUSOIDAL WAVES FROM BINARIES. FOURIER ANALYSIS.

It is generally assumed that galactic and extragalactic binary systems are the most promising sources of gravitational waves for detectors based on laser interferometry. In fact, waves from a binary star, including the effect of eccentricity, orbital inclination, and also post-Newtonian corrections, have long been studied, and are today well understood. In

particular, the sensitivity of the planned space interferometers should allow the detection of waves from several known galactic binary stars. In the LISA and OMEGA frequency band, the strongest among these sources are presumably the Interacting White Dwarfs Binaries (IWDB) [8,9]. Table I contains the available data for five IWDB, including the amplitude and frequency of the expected gravitational waves. We have applied our results to these objects, and describe the LISA's response to the waves originating from them. Fig. 11 shows the beam-pattern factors  $F_+$  and  $F_\times$  for the five IWDB in Table I, as seen from LISA over one year. Fig. 11 also shows the analogous quantities for a sinusoidal signal, of unspecified amplitude and frequency, coming from the galactic centre.

We will now consider the effect of the motion in the frequency domain, for both the space-born and the terrestrial cases. We define the Fourier series as usual

$$P(t) = a_0 + \sum_{k=1}^{\infty} \left\{ a_k \cos\left(\frac{k\pi t}{L}\right) + b_k \sin\left(\frac{k\pi t}{L}\right) \right\}, \quad (27)$$

where  $T = 2L$  is the orbital period, and

$$a_0 = \frac{1}{2L} \int_{-L}^{+L} P(t) dt, \quad (28)$$

$$a_k = \frac{1}{L} \int_{-L}^{+L} P(t) \cos\left(\frac{k\pi t}{L}\right) dt, \quad (29)$$

$$b_k = \frac{1}{L} \int_{-L}^{+L} P(t) \sin\left(\frac{k\pi t}{L}\right) dt. \quad (30)$$

For the conical case analyzed in Sec. III, using eqs.(B1)-(B14) of Appendix B, one finds that the only non-zero Fourier coefficients are given by ( $\delta_0 \equiv \phi - \eta_0$ ,  $k = 1, \dots, 8$ ):

$$a_0 = \lambda_0 + \frac{1}{2}(\mu_4 + \sigma_4) \cos[4(\delta_0 - \xi_0)], \quad (31)$$

$$\begin{aligned} a_k = & \mu_0 \cos(4\xi_0) \delta_{k4} + \sum_{n=1}^4 \left\{ \lambda_n \cos(n\delta_0) \delta_{nk} \right. \\ & + \frac{1}{2}(\mu_n + \sigma_n) \cos(n\delta_0 - 4\xi_0) \delta_{k+n,4} \\ & \left. + \frac{1}{2}(\mu_n - \sigma_n) \cos(n\delta_0 + 4\xi_0) \delta_{k-n,4} \right\}, \end{aligned} \quad (32)$$

$$\begin{aligned} b_k = & \mu_0 \sin(4\xi_0) \delta_{k4} + \sum_{n=1}^4 \left\{ \lambda_n \sin(n\delta_0) \delta_{nk} \right. \\ & - \frac{1}{2}(\mu_n + \sigma_n) \sin(n\delta_0 - 4\xi_0) \delta_{k+n,4} \\ & \left. + \frac{1}{2}(\mu_n - \sigma_n) \sin(n\delta_0 + 4\xi_0) \delta_{k-n,4} \right\}. \end{aligned} \quad (33)$$

The analogous calculation for the terrestrial case, described by Eqs. (24), gives the following nine coefficients ( $k = 1, \dots, 4$ )

$$a_0 = \lambda_0 + \mu_0 \cos(4\iota), \quad (34)$$

$$a_k = [\lambda_k + \mu_k \cos(4\iota)] \cos(k\delta_0) + \sigma_k \sin(4\iota) \sin(k\delta_0), \quad (35)$$

$$b_k = [\lambda_k + \mu_k \cos(4\iota)] \sin(k\delta_0) - \sigma_k \sin(4\iota) \cos(k\delta_0). \quad (36)$$

In general, given the initial detector's position, these Fourier coefficients depend on the source's coordinates  $\theta$  - through  $\lambda_k, \mu_k, \sigma_k$  - and  $\phi$  - through  $\delta_0$ . If the source location is known, then one can look for these spectral lines as a convincing signature about the gravitational origin of the signal. When the source's coordinates are unknown, however, one has to deal with the complication arising from the Doppler effect [11]. The motion of the detector, besides the amplitude modulation described in the present work, also introduces a location-dependent phase modulation, in the form of a Doppler broadening of the sinusoidal signal. In the case of LISA, the magnitude of this effect, over a period  $T = 1$  yr, is

$$\frac{\Delta f}{f} \simeq 2 \times 10^{-4}, \quad (37)$$

so that, in the spectral region below  $10^{-2}$  Hz, we do not have any hope of finding the aforementioned lines, separated from each other by only  $1/T \simeq 3 \times 10^{-8}$  Hz. For a terrestrial interferometer, the situation is analogous, only complicated by the simultaneous effects of the diurnal and annual motion of the earth, and also by the earth-moon interaction.

In conclusion, for long enough observations, we need special techniques to compensate for the frequency spread over several frequency-resolution bins, and eventually to recover the amplitude modulation described in this paper. Several different strategies can be adopted to overcome this problem, although none of them is completely satisfactory, due to the large amount of computation involved. See [11] for more details. In any case, the amplitude modulation can be exploited for an independent measurement of the location of the source, and, in addition, to obtain the polarization of the wave.

## VI. CONCLUSIONS

In the present work, we have considered a gravitational wave interferometer, in motion with respect to fixed stars, and studied the resulting amplitude modulation of a long-duration continuous signal. The general results are presented in Sec. II, where the instantaneous beam-pattern factors - Eqs. (11) - and the polarization-averaged antenna power pattern - Eq. (12) - are given as functions of time, for a generic motion.

Next, two particular cases have been analyzed: 1) the probable orbit of a space-born interferometer, with particular emphasis on LISA, and 2) the motion of a ground-based interferometer.

For what concerns LISA, we have shown that its peculiar motion makes the time-averaged antenna pattern practically isotropic, thus providing an uniform coverage of the whole sky over the period of one year. For shorter integration periods directionality is mostly preserved, and can be exploited where necessary, for example in the search of a galactic binaries background. However, when we focused on the galactic disk, we found that the average antenna response is far from optimal, due to the relative orientation of the Ecliptic and the galactic plane itself. We stress that these results are not conclusive, since we have neglected the

anisotropy in the distribution of the sources with respect to the sun, due to the fact that we are located near the edge of the disk. In this respect, additional work is needed.

In the terrestrial case, thanks to the probable redundancy of future gravitational wave observatories, the discussion about a single antenna's sky's coverage is not so critical. However, we found that there are particular positions on the earth's surface, given in Eqs. (26), which render the time-averaged antenna response perfectly isotropic. For what concerns the galactic plane, since the latter makes with the Equatorial plane approximately the same angle it makes with the Ecliptic ( $\sim 60^\circ$ ), the result is analogous to the conical case, with the angle  $\zeta$  interpreted as  $90 - \ell$  in Fig. 9. In other words, the response to the galactic plane increases as we move the interferometer from the equator toward the poles, with a minor role played by the orientation angle  $\iota$ .

### ACKNOWLEDGMENTS

The author would like to thank P.Bender and R.Hellings for discussions. The research described in this paper was performed while the author held an NRC-NASA Resident Research Associateship at the Jet Propulsion Laboratory, California Institute of Technology, under a contract with the National Aeronautics and Space Administration.

### APPENDIX A:

In this Appendix, we give the coefficients  $A, B, C$ , and  $D$  which enter in the expressions of  $F_+$  and  $F_\times$ , Eqs. (11). They, in turn, can be expressed in terms of intermediate quantities  $\alpha_1, \alpha_2, \beta_1$ , and  $\beta_2$  as follows

$$A = \alpha_1\beta_1 + \alpha_2\beta_2 \tag{A1}$$

$$B = \alpha_1\beta_2 - \alpha_2\beta_1 \tag{A2}$$

$$C = \frac{1}{2} [\beta_1^2 - \beta_2^2 - \alpha_1^2 + \alpha_2^2] \tag{A3}$$

$$D = \alpha_1\alpha_2 + \beta_1\beta_2 \tag{A4}$$

where

$$\alpha_1 = \cos \delta$$

$$\alpha_2 = \cos \theta \sin \delta$$

$$\beta_1 = \cos \zeta \sin \delta$$

$$\beta_2 = \cos \zeta \cos \theta \cos \delta + \sin \zeta \sin \theta$$

### APPENDIX B:

In this Appendix, we give the coefficients  $\lambda_n, \mu_n$ , and  $\sigma_n$  ( $n = 0, \dots, 4$ ), defined in Eq. (12), as functions of the angles  $\theta$  and  $\zeta$ .

$$\lambda_0 = \frac{1}{64} \left( 35 + 35 \cos^4 \theta \cos^4 \zeta - 30 \cos^2 \theta + 3 \cos^4 \zeta + 108 \cos^2 \zeta \cos^2 \theta \right. \\ \left. - 30 \cos^2 \zeta \cos^4 \theta - 30 \cos^4 \zeta \cos^2 \theta - 30 \cos^2 \zeta + 3 \cos^4 \theta \right) \quad (\text{B1})$$

$$\lambda_1 = \frac{1}{32} \sin(2\zeta) \sin(2\theta) \left( 15 - 3 \cos^2 \theta - 3 \cos^2 \zeta + 7 \cos^2 \zeta \cos^2 \theta \right) \quad (\text{B2})$$

$$\lambda_2 = \frac{1}{16} \left( 7 + 7 \cos^4 \theta \cos^4 \zeta - 8 \cos^2 \theta + \cos^4 \zeta + 16 \cos^2 \zeta \cos^2 \theta - 8 \cos^2 \zeta \cos^4 \theta \right. \\ \left. - 8 \cos^4 \zeta \cos^2 \theta - 8 \cos^2 \zeta + \cos^4 \theta \right) \quad (\text{B3})$$

$$\lambda_3 = \frac{1}{8} \sin^3 \zeta \cos \zeta \sin^3 \theta \cos \theta \quad (\text{B4})$$

$$\lambda_4 = \frac{1}{64} \sin^4 \zeta \sin^4 \theta \quad (\text{B5})$$

$$\mu_0 = -\frac{1}{64} \sin^4 \zeta \left( 3 - 30 \cos^2 \theta + 35 \cos^4 \theta \right) \quad (\text{B6})$$

$$\mu_1 = -\frac{1}{16} \sin(2\theta) \cos \zeta \sin^3 \zeta \left( 3 - 7 \cos^2 \theta \right) \quad (\text{B7})$$

$$\mu_2 = \frac{1}{16} \sin^2 \zeta \sin^2 \theta \left( 1 + \cos^2 \zeta \right) \left( 1 - 7 \cos^2 \theta \right) \quad (\text{B8})$$

$$\mu_3 = \frac{1}{16} \sin(2\zeta) \sin^3 \theta \cos \theta \left( 3 + \cos^2 \zeta \right) \quad (\text{B9})$$

$$\mu_4 = -\frac{1}{64} \sin^4 \theta \left( 1 + \cos^4 \zeta + 6 \cos^2 \zeta \right) \quad (\text{B10})$$

$$\sigma_0 = 0 \quad (\text{B11})$$

$$\sigma_1 = -\frac{1}{16} \sin(2\theta) \sin^3 \zeta \left( 3 - 7 \cos^2 \theta \right) \quad (\text{B12})$$

$$\sigma_2 = \frac{1}{8} \cos \zeta \sin^2 \zeta \sin^2 \theta \left( 1 - 7 \cos^2 \theta \right) \quad (\text{B13})$$

$$\sigma_3 = \frac{1}{8} \sin \zeta \cos \theta \sin^3 \theta \left( 1 + 3 \cos^2 \zeta \right) \quad (\text{B14})$$

$$\sigma_4 = -\frac{1}{16} \sin^4 \theta \cos \zeta \left( 1 + \cos^2 \zeta \right) \quad (\text{B15})$$

### APPENDIX C:

In this Appendix, we provide the coefficients  $\lambda_n$ ,  $\mu_n$ , and  $\sigma_n$  ( $n = 0, \dots, 4$ ) for LISA

$$\lambda_0 = \frac{1}{1024} \left( 443 - 37 \cos^4 \theta - 78 \cos^2 \theta \right) \quad (\text{C1})$$

$$\lambda_1 = \frac{\sqrt{3}}{256} \sin(2\theta) \left( 57 - 5 \cos^2 \theta \right) \quad (\text{C2})$$

$$\lambda_2 = \frac{9}{256} \left( 9 - \cos^4 \theta - 8 \cos^2 \theta \right) \quad (\text{C3})$$

$$\lambda_3 = \frac{3\sqrt{3}}{128} \sin^3 \theta \cos \theta \quad (\text{C4})$$

$$\lambda_4 = \frac{9}{1024} \sin^4 \theta \quad (\text{C5})$$

$$\mu_0 = -\frac{9}{1024} (3 + 35 \cos^4 \theta - 30 \cos^2 \theta) \quad (\text{C6})$$

$$\mu_1 = -\frac{3\sqrt{3}}{256} \sin(2\theta) (3 - 7 \cos^2 \theta) \quad (\text{C7})$$

$$\mu_2 = \frac{15}{256} \sin^2 \theta (1 - 7 \cos^2 \theta) \quad (\text{C8})$$

$$\mu_3 = \frac{13\sqrt{3}}{128} \sin^3 \theta \cos \theta \quad (\text{C9})$$

$$\mu_4 = -\frac{41}{1024} \sin^4 \theta \quad (\text{C10})$$

$$\sigma_0 = 0 \quad (\text{C11})$$

$$\sigma_1 = -\frac{3\sqrt{3}}{128} \sin(2\theta) (3 - 7 \cos^2 \theta) \quad (\text{C12})$$

$$\sigma_2 = \frac{3}{64} \sin^2 \theta (1 - 7 \cos^2 \theta) \quad (\text{C13})$$

$$\sigma_3 = \frac{7\sqrt{3}}{64} \sin^3 \theta \cos \theta \quad (\text{C14})$$

$$\sigma_4 = -\frac{5}{128} \sin^4 \theta \quad (\text{C15})$$

## REFERENCES

- [1] F.B. Estabrook and H.D. Wahlquist, *Gen. Rel. Grav.* **6**, 439 (1975).
- [2] K. Danzmann et al., *LISA: Proposal for a Laser Interferometric Gravitational Wave Detector in Space*, Report No. MPQ 177, Max-Planck Institut für Quantenoptik (Garching bei München, Germany, 1993); P.L. Bender et al., *LISA: Presentation of Assessment Study Results*, ESA SCI(94)9 (1994).
- [3] J. Hough et al., in *First Edoardo Amaldi Conference on Gravitational Wave Experiments* (World Scientific, Singapore, 1995).
- [4] R.W. Hellings et al., *OMEGA: Orbiting Medium Explorer for Gravitational Astrophysics*, Midex Proposal (Jet Propulsion Laboratory, 1995).
- [5] K.S. Thorne, in *300 Years of Gravitation*, eds. S.W. Hawking and W. Israel (Cambridge University Press, Cambridge, 1987); see also S.V. Dhurandhar and M. Tinto, *M.N.R.A.S.* **234**, 663 (1988).
- [6] G. Giampieri, R.W. Hellings, M. Tinto, and J.E. Faller, *Optics Comm.* **123**, 669 (1996).
- [7] R.W. Hellings, G. Giampieri, L. Maleki, M. Tinto, K. Danzmann, J. Hough, and D. Robertson, *Optics Comm.* **124**, 313 (1996).
- [8] C.R. Evans, I. Iben, and L. Smarr, *Astrophys. J.* **323**, 129 (1987).
- [9] D. Hils, P.L. Bender, and R.F. Webbink, *Astrophys. J.* **360**, 75 (1990).
- [10] B.F. Schutz and M. Tinto, *M.N.R.A.S.* **224**, 131 (1987).
- [11] B.F. Schutz, in *The Detection of Gravitational Waves*, ed. D.G. Blair (Cambridge University Press, Cambridge, 1991).

## FIGURES

FIG. 1. The geometry of the interferometer. Note that the usual spherical polar coordinates of the source's position are  $(\theta, \phi - \pi/2)$ .

FIG. 2. OMEGA: a space-born detector rotating around its vertical axis. Although the actual OMEGA's motion is better described with the formalism introduced in Sec. III, this simple example can provide a good approximation to it.

FIG. 3. The relation between the wave's  $(X, Y, Z)$ , the detector's  $(x, y, z)$ , and the fixed  $(x', y', z')$  reference frames.

FIG. 4. LISA: a space-born interferometer in orbit around the sun. Reproduced from [3], with permission.

FIG. 5. The antenna pattern, averaged over time and polarization, for various values of the inclination angle  $\zeta$ . a)  $\zeta = 0$ . b)  $\zeta = 30^\circ$ , c)  $\zeta = 60^\circ$ , d)  $\zeta = 90^\circ$ . LISA corresponds to case c).

FIG. 6. The  $\phi$ -dependence on the Ecliptic plane, as a function of the angle  $\zeta$ . The bigger is the difference between  $\lambda_0$  and  $|\mu_4 + \sigma_4|/2$ , the smaller is the dependence on the direction  $\phi$  in the averaged antenna pattern.

FIG. 7. The r.m.s. deviation from isotropy of the time-averaged antenna pattern, as a function of  $\zeta$ . The minimum of  $\Delta$  corresponds to the maximum attainable isotropic response. This minimum occurs at  $\zeta \simeq 55^\circ$ , for which  $\Delta \simeq 0.08$ . For LISA,  $\Delta(60^\circ) \simeq 0.14$ .

FIG. 8. LISA's antenna pattern averaged over (a) 3 months and (b) 6 months. The initial conditions are  $\xi_0 = \eta_0 = 0$ .

FIG. 9. The response of a space interferometer to the galactic disk, as a function of the angle  $\zeta$ . For simplicity, a small dependence on the detector's initial orientation, more precisely on  $\eta_0 + \xi_0$ , has been neglected.

FIG. 10. The minimum r.m.s. deviation from isotropy  $\Delta_*$  attainable at any given latitude. The corresponding optimal orientation  $\iota_*$  is also shown.

FIG. 11. The LISA normalized responses to the 5 IWDB systems shown in Table I, and to a hypothetical source in the galactic center, over one year of observations. The two curves give the beam-pattern factors  $F_+$  (solid line) and  $F_\times$  (dashed line). We have assumed the initial conditions  $\xi_0 = \eta_0 = 0$ , and a polarization angle  $\psi = 2$ . Horizontal axis is time in years.

## TABLES

TABLE I. Data for 5 known IWDB. The first column is the name, the second and third column are, respectively, the angles  $\theta$  and  $\phi$  in the Ecliptic coordinate system. The last two columns gives, respectively, the predicted amplitude and frequency of the gravitational waves.

Name	$\theta$ (degrees)	$\phi$ (degrees)	GW Amplitude ( $10^{-22}$ )	GW Frequency ( $10^{-3}$ Hz)
<i>AM CVn</i>	52.56	260.38	5.27	1.94
<i>CR Boo</i>	72.10	292.27	2.82	1.34
<i>V803 Cen</i>	120.31	306.17	0.89	1.24
<i>CP Eri</i>	120.83	151.77	4.02	1.16
<i>GP Com</i>	67.00	277.73	1.77	0.72

Figure 1

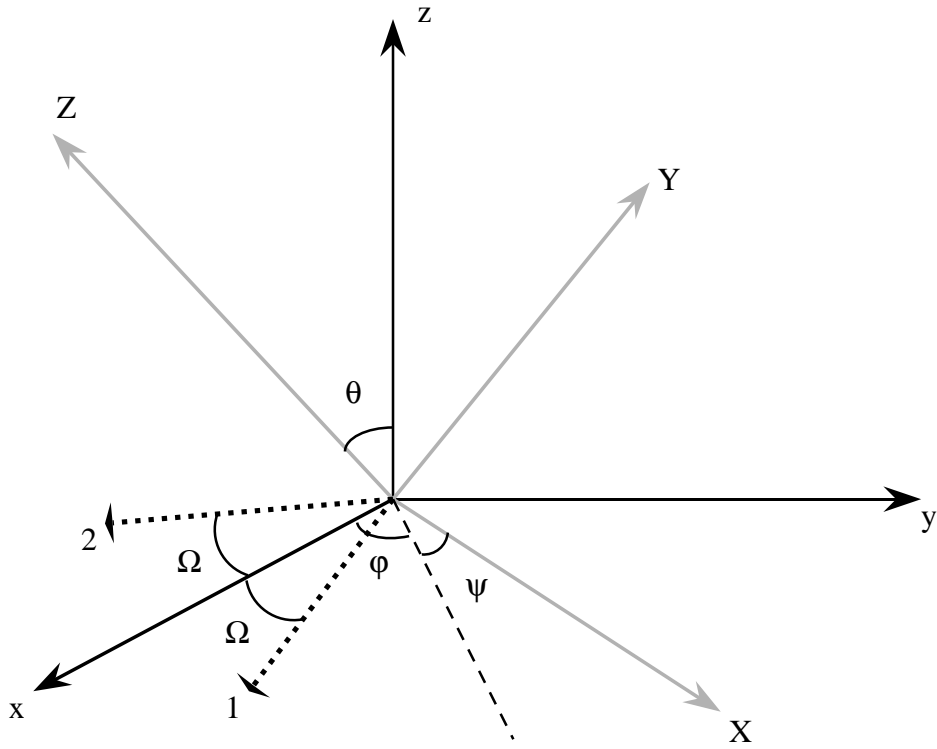


Figure 2

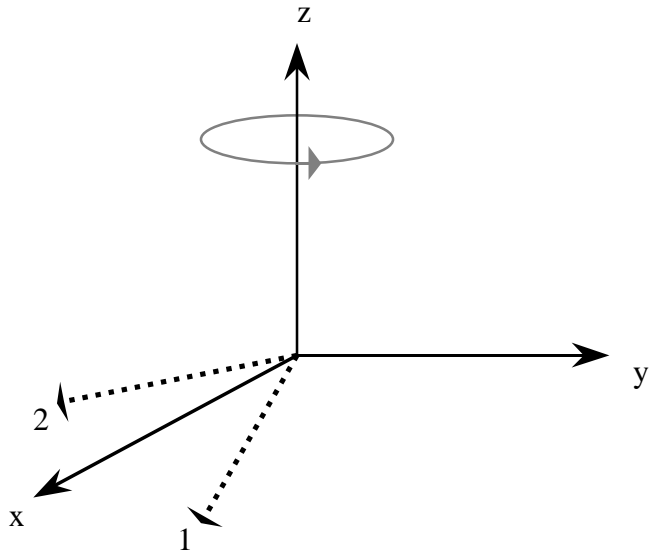
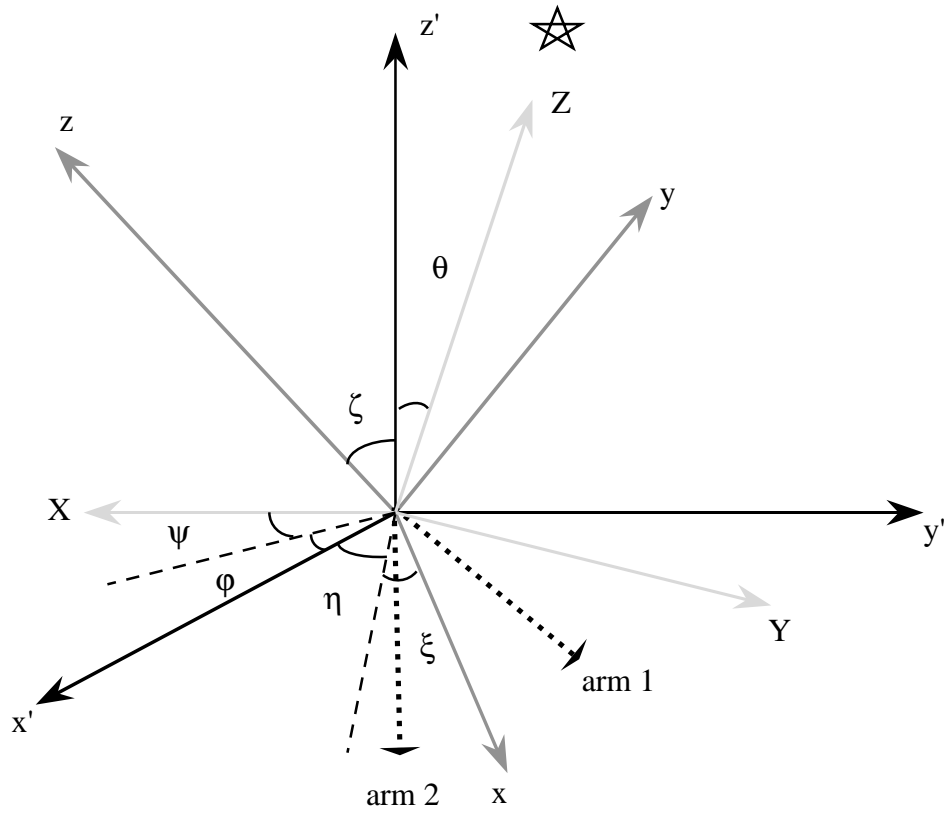


Figure 3



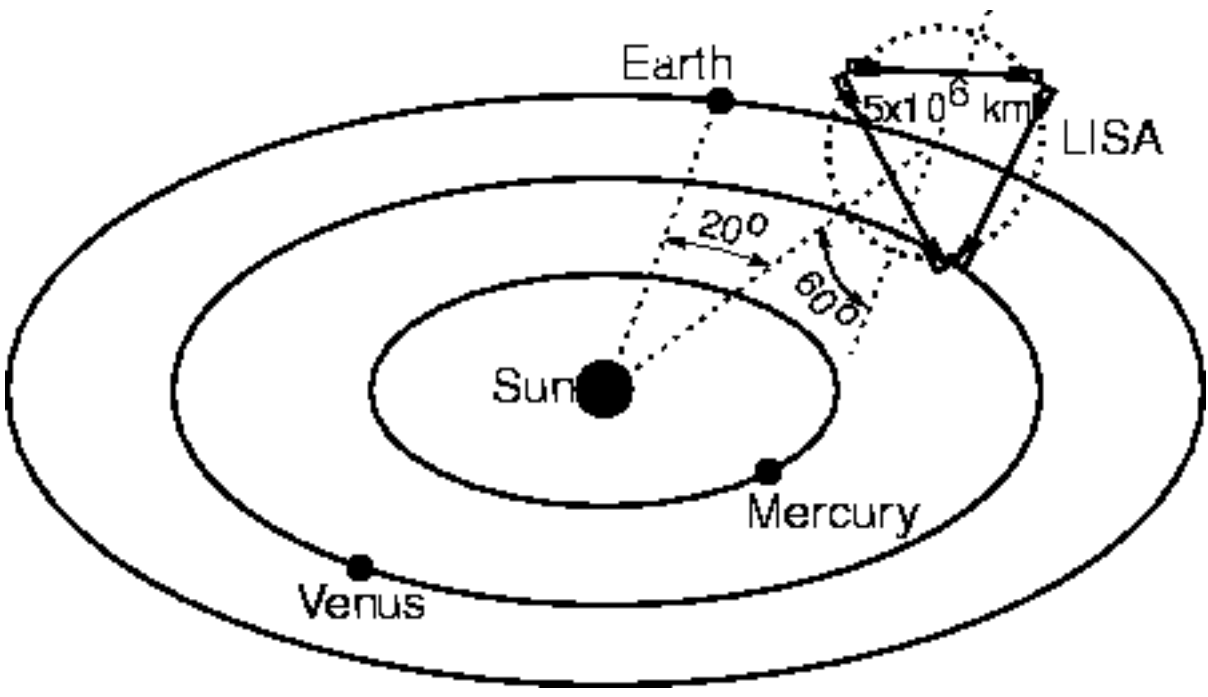
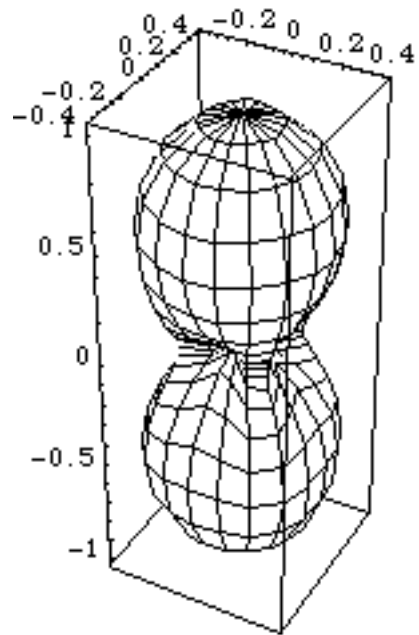
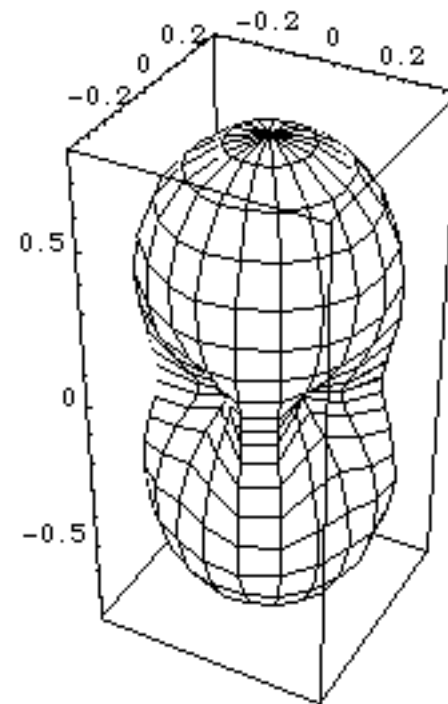


Fig. 5a



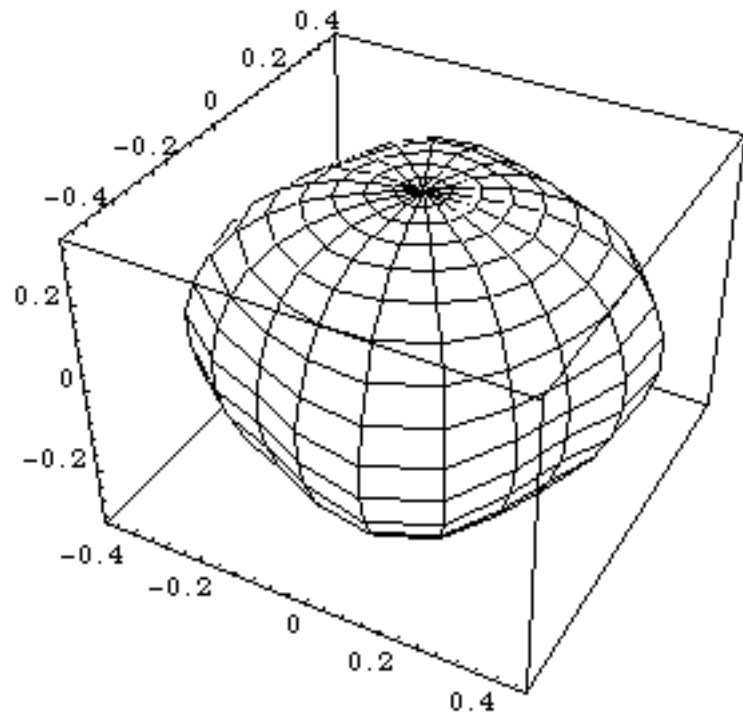
$$\zeta=0$$

Fig. 5b



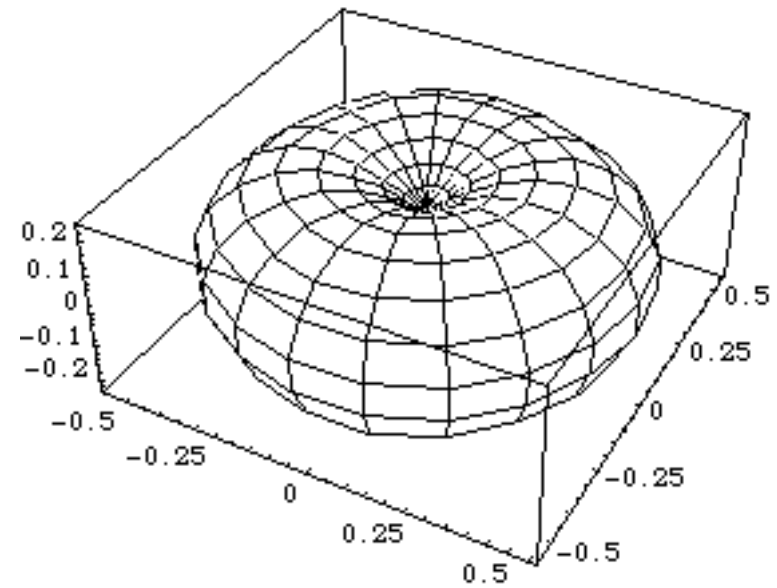
$$\zeta=\pi/6$$

Fig. 5c



$$\zeta = \pi/3$$

Fig. 5d



$$\zeta = \pi/2$$

Figure 6

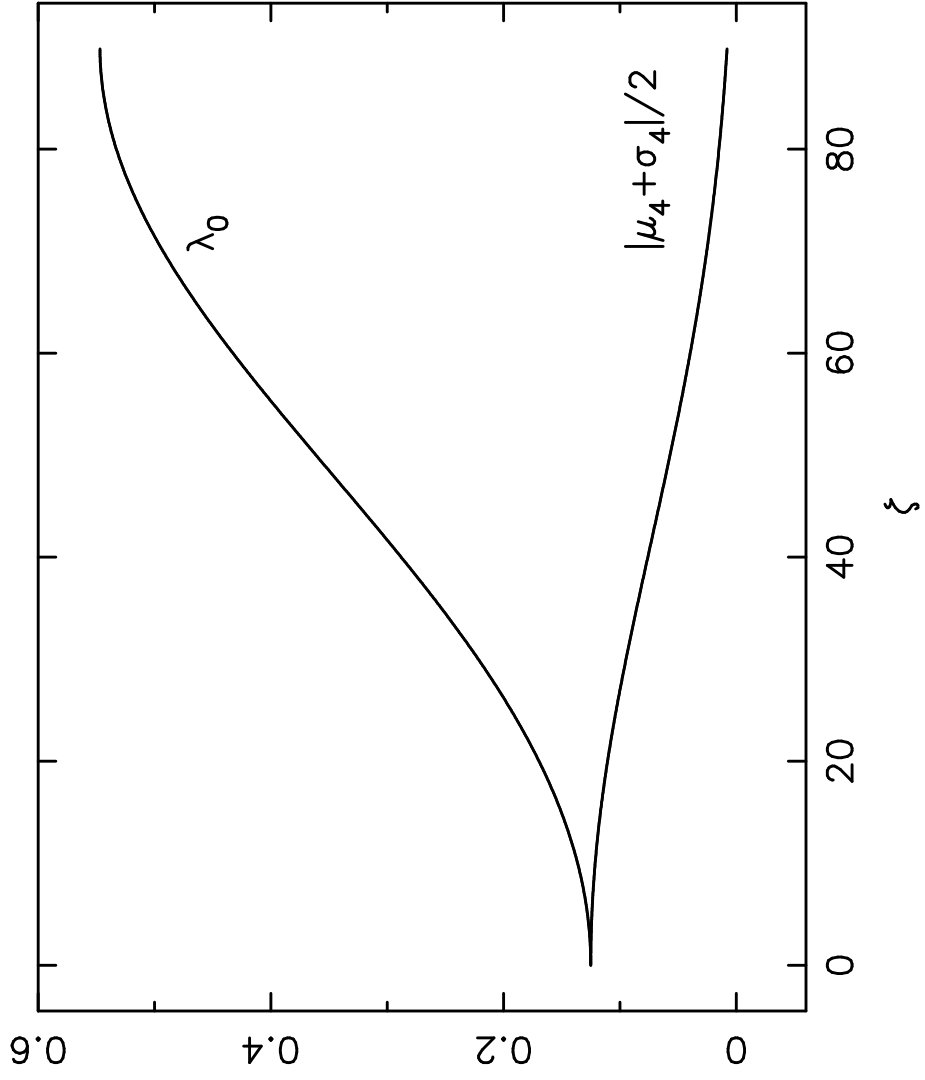


Figure 7

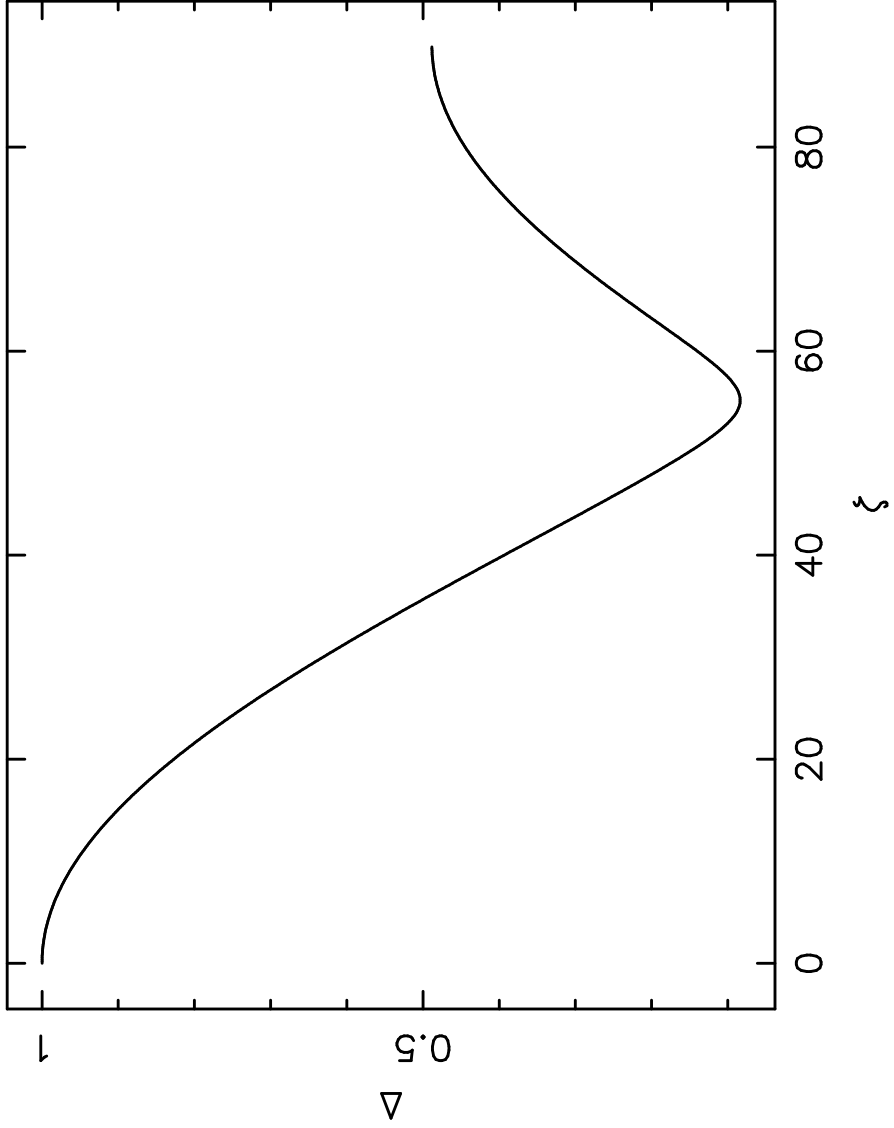
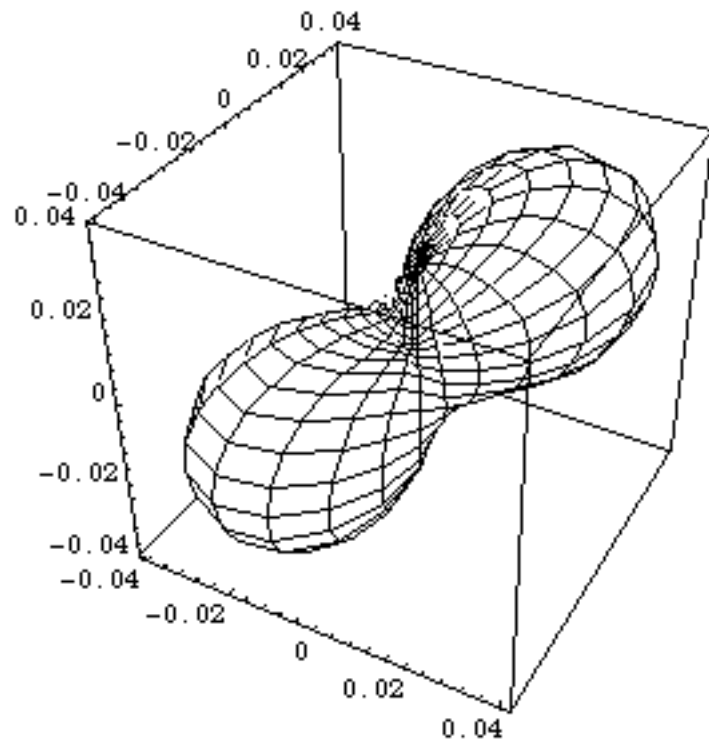
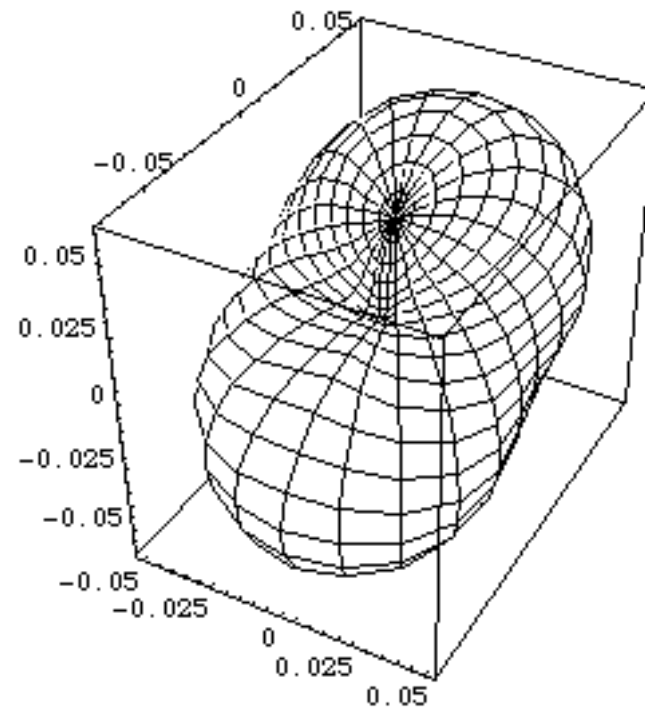


Fig. 8a



3 months average

Fig. 8b



6 months average

Figure 9

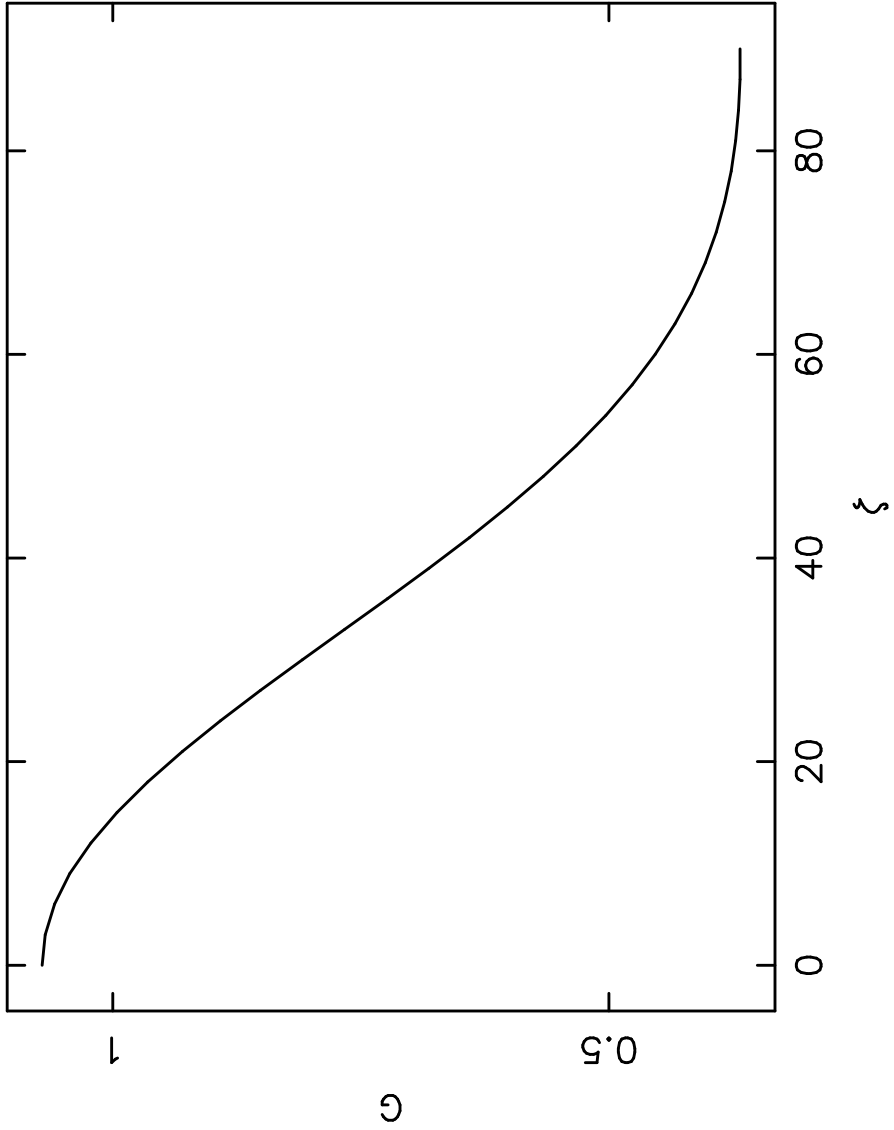
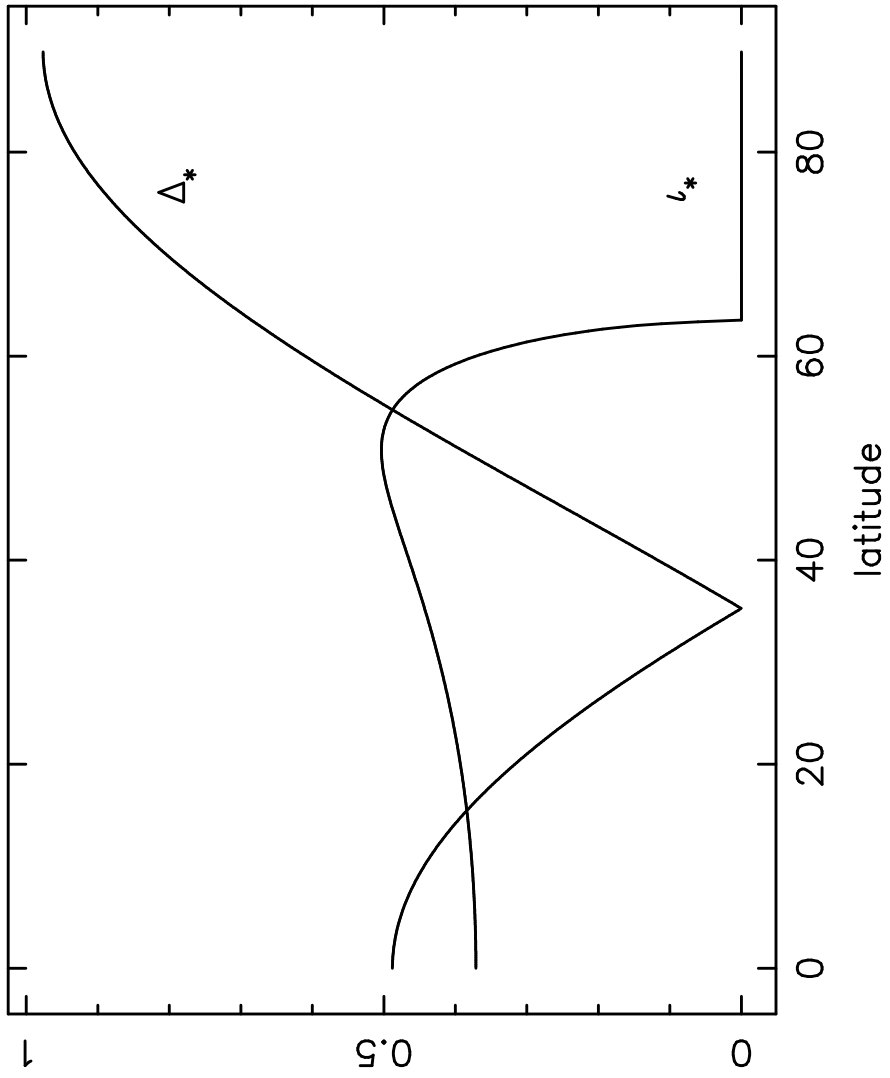
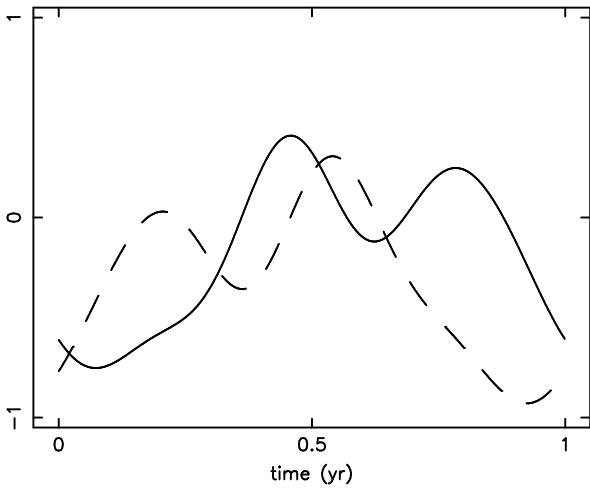


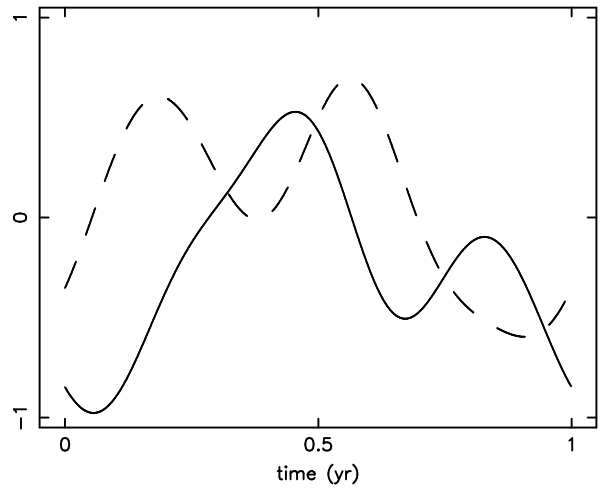
Figure 10



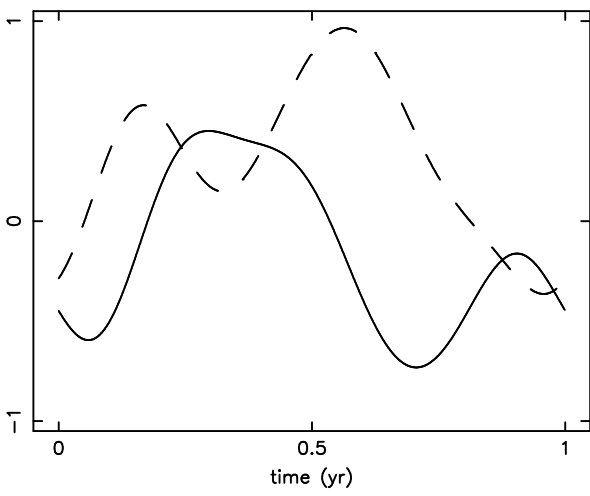
AM CVn



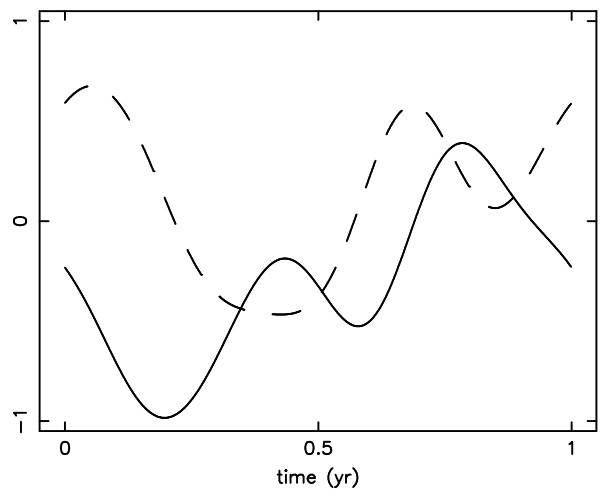
CR Boo



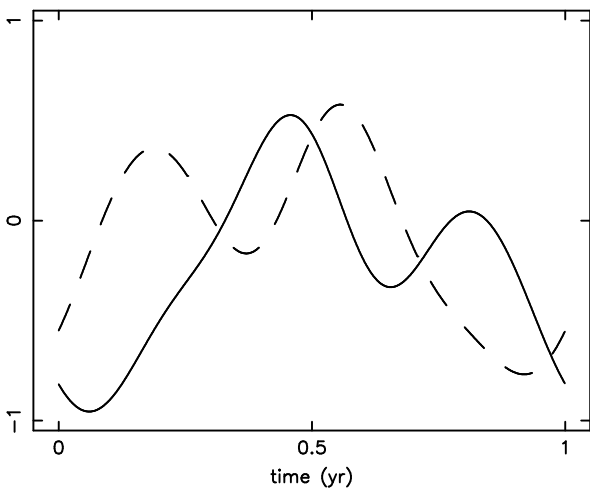
V803 Cen



CP Eri



GP Com



Galactic Center

